Indian Journal of Chemical Technology
Vol. 31, March 2024, pp. 197-212
DOI: 10.56042/ijct.v31i2.4738

Exact solutions on magnetohydrodynamic Casson nanofluid EG-GO and EG-MWCNT over a vertical plate with shape factors: Caputo fractional derivative

N Jyothi & A G Vijayakumar*

Department of Mathematics, Vellore Institute of Technology, Vellore-632 014, Tamil Nadu, India

*E-mail: vijayakumarag@vit.ac.in

Received 9 August 2023; accepted 12 February 2024

The aim of the present work is to apply the Caputo-fractional derivative to the heat transformation of unsteady incompressible magnetohydrodynamic (MHD) Casson nanofluid flow. Ethylene Glycol-Graphene oxide and Ethylene glycol-Multiwall Carbon nanotubes considered as nanofluids. The current study helps in understanding the fluid dynamics involved in water purification, energy conservation, solar energy, coolants, cancer therapies, and physiological fluid dynamics. By using appropriate non-dimensional variables, the leading PDE of the problem are non dimensionalized. The governing equations are solved by the combined integral transforms of Fourier sine and Laplace transform technique. For an extensive study of the problem, graphical illustrations and tables are developed by using the MATLAB software. The effects of the order of the Caputo derivative, thermal Grashof number, viscous dissipation, and Casson parameter oscillations on the fractional heat and momentum equations are inspected. The thermal and velocity profiles are increased for thermal Grashof number and Casson parameter. Symmetry phenomena are also observed in the case of cooling and heating plate for thermal Grashof number. Different shapes of nanoparticles are performed for ordinary fractional parameters which is increased for temperature as well as velocity.

Keywords: Caputo fractional derivative, Casson fluid, Magnetohydrodynamics, Mittag-Leffler fractional operator, nanoparticle shape factor

Introduction

In recent era, the fractional calculus (FC) became very popular. This is providing tremendous progress in many areas of sciences and an active area of development. Previous years FC is using in only mathematics but last three decades onwards it is variously using in many disciplines for instance, physics, bioengineering, Chaos theory, electromagnetism, economics and finance, many Others[1-7]. There are many definitions of FC have been proposed for instant: Grunwald-Letnikov, Riemann-Liouville, Caputo, Caputo-Febrizio, Atangana-Baleanu and Prabhakar's fractional approach[8-15]. Fractional order systems can process efficient information, improving the simulations of the integer order systems and also provide most accurate results. There exists a lot of numerical and analytical methods already developed to solve highly complex fractional order derivative equations. For example, homotopy-perturbation method[16], Adams-Bashfort-Moulton method[17], Iterative sequence technique[18], Adomian decomposition method[19], Laplace transform technique[20], Residual power series method[21], Fourier Sine transform method[22], and others[23-26].

In modern years, nanotechnology is playing a vital role in every discipline. fluids and nanofluids models are attracting many researchers. Nanofluid is a mixture of pure fluids (water, alcohol, kerosene, oil, Ethylene glycol, etc.,) and nanometer sized particles (Cu, Ag, GO, Gr, Al_2O_3, etc.,)[27]. Nanofluids show enhanced characteristics of heat conductivity in comparison with the convectional nanofluids flows and hence are very much important in industrial fields. Heat transformation is not only a technical issue where it is important there is a challenge for engineers and industrial people. Nanofluids are the best solution to heat transfer related problems. Nanoparticles also give the outstanding results in medical sciences, for instance, diagnosis process, drug delivery, artificial lungs, laser treatments, heat deceases, hyperthermia, cancer treatment, among others[28]. Generally, shapes, size of nanoparticles, volume of the proportion and base fluids help us to establish the general performance and usefulness of nanofluids[29].

The study of how magnetic fields and fluid conductors interact is known as magnetohydro-

dynamics (MHD). There are several uses for the MHD nanofluids in wavelength filters since they contain both magnetic and liquid characteristics. For example, MHD traditionally describes macroscopic force balance, Solar wind, Drug delivery for cancer therapy, optical materials (nonlinear), optical gratings, ink float separation, optical switches, magneto-optical systems, etc. Another significant use of MHD is the separation of non-metallic materials from metals with high melting points[30]. Khalid et al.[31] have studied the unsteady free convective MHD Casson fluid flow over an oscillating porous vertical plate. Bhatta et al.[32] have studied optically thick radiating free convective MHD nanofluid flow over an exponentially accelerated plate. Many research articles dealing with modelling fluid models with fractional operator. Hanifa and Shafie described the application in petroleum industry as the aluminium trioxide (Al_2O_3) impact in electrically conducting mineral oil-based fractional Maxwell nanofluid[33]. Sene[34] used the analytical investigations to solve the second grade fluid with Newtonian heating under Caputo fractional derivative. Anwar et al.[35] solved the fractional nonlinear PDEs numerically via finite-difference discretization along with L1 algorithm. Gohar Ali et al.[36] proposed the Casson fluid flowing in a two-phase generalised MHD free convection between parallel plates. Arif et al.[37] proposed the solution of generalized Couette Flow for fractional model of couple stress fluid. Souayeh et al. [38] used the Fourier sine transform method and solved the governing equations for thermal characteristics with Fourier and non-Fourier heat transfer. Zubair et al.[39] investigated unsteady free convection nanofluid flow of viscous fluids through an isothermal vertical sheet. Fatima et al.[40] studied the influence of heat and mass transmission on different types of nanofluids with CNTs of fractional order derivatives. Significant analytical investigations on the chemical and thermal effects on magneto hydrodynamics Casson fluids of Caputo-Fabrizio fractional order derivative was discussed by Reyaz et al.[41]. Few relevant studies are shown in other published papers[42-45].

To the author's best knowledge MHD, comparison between two nanofluids with shape effects has not been investigated. Present work is an extension of the study by NdoleneSene work. With the use of the Caputo fractional derivative (CFD) approach, the primary goal of the present work is to examine the flow of Casson nanofluids with form effects over an infinite vertical surface. The solution process is followed by the combination of Fourier sine and Laplace transform techniques. Using the mathematical programme MATLAB, the flow parameter data are displayed graphically and numerically with physical demonstrations. In this paper, we consider Ethylene glycol as host fluid and Graphene oxide and MWCNT's are spherical shaped Casson nanoparticles.

Preliminary definitions

In this section, fractional order operators known as Riemann-Liouville integral, Caputo derivative and some special functions are given. The Caputo derivative and its Fourier sine and Laplace Transforms helped us to obtain exact analytical solutions for the constructive equations. To reach the solution, we begin this part by Mittag-Leffler kernel function definition, which has two arguments. The structure of the precise solution to the FDE is significantly influenced by this peculiar function.

Definition 1:[11] Let $\alpha > 0, \beta \in \mathbf{R}$ and $Z \in C$. The definition of the Mittag-Leffler function is

[

$$E_{\alpha,\beta}(Z) = \sum_{k=0}^{\infty} \frac{Z^k}{\Gamma(\alpha k + \beta)}$$

When $\alpha > 0$ and $\beta > 0$, the Convergent series.

If $\beta = 1$, We discover the Erdelyi-introduced Mittag-Leffler function, which is defined as

$$E_{\alpha,1}(Z) = \sum_{k=0}^{\infty} \frac{Z^k}{\Gamma(1+\alpha k)}$$

If $\alpha = \beta = 1$ we obtain the following relationships

$E_{\alpha,1}(Z) = E_{\alpha}(Z)$ $\quad$ $E_{1,1}(Z) = E_1(Z) = \exp(Z).$

Definition 2:[10,11] The Riemann–Liouville integral of examine function υ: $\upsilon : [0, +\infty[\to R$ can be written as:

$$\left(I^{\alpha}\upsilon\right)(t) = \frac{1}{\Gamma(\alpha)} \int_0^t (t-s)^{\alpha-1} \nu(s)\, ds$$

Where $\Gamma(\alpha)$ is the Gamma function and with fractional order α verify the condition ($\alpha > 0$). Next we recall the Caputo fractional operator. Further investigations of the problem we use this fractional operator and its association with Fourier sine and

Laplace transformation. The main reason of using this derivative is that obeys the initial conditions consider in the present investigation opposed to the Riemann–Liouville derivative, the reason for using the initial conditions in an integral notation that cannot be physically interpreted.

Definition 3:[10,11] define the Riemann-Liouville derivative of examine function $\upsilon:[0,+\infty[\to R$, of order α as in the representing form:

$$D^{\alpha}\upsilon(t)=\frac{1}{\Gamma(1-\alpha)}\frac{d}{dt}\int_0^t \upsilon(s)(t-s)^{-\alpha}ds$$

Where time $t>0$, the order of the fractional operator verify the assumption that $\alpha\in(0,1)$ and $\Gamma(...)$ indicates the Euler's Gamma function .

Definition 4:[10,11] define the Caputo fractional operator of the given function $\upsilon:[0,+\infty[\to R$, of order α is in the form:

$$D_C^{\alpha}\upsilon(t)=\frac{1}{\Gamma(1-\alpha)}\int_0^t \frac{d\upsilon(s)}{ds}(t-s)^{-\alpha}ds$$

Where time $t>0$, the order of the fractional operator verify the assumption that $\alpha\in(0,1)$ and $\Gamma(1-\alpha)$ indicates the Euler's Gamma function.

The ODEs, PDEs, fractional operators and the Laplace and Fourier transforms play vital role in our investigations. To determine the analytical solutions, we use Laplace transform. In this paper, besides it, used the Fourier sine transform. The Laplace transform of the Caputo fractional derivative[10,11] is represented as the following form

$$L\left\{D_C^{\alpha}\upsilon(t)\right\}=s^{\alpha}L\left\{\upsilon(t)\right\}-s^{\alpha-1}\upsilon(0)$$

Where the fractional operator α obeys the relationship $\alpha\in(0,1)$.

Fractional mathematical formulation for Caputo derivative[29,49]

The constructive equations presented here the subject of investigations. The current flow mechanism considered as incompressible, unsteady, MHD flow of Casson nanofluid involving of nanoparticles through an infinite vertical plate. Fig. 1 considers fluid motion along the x-axis and y-axis to be normal to the plate.

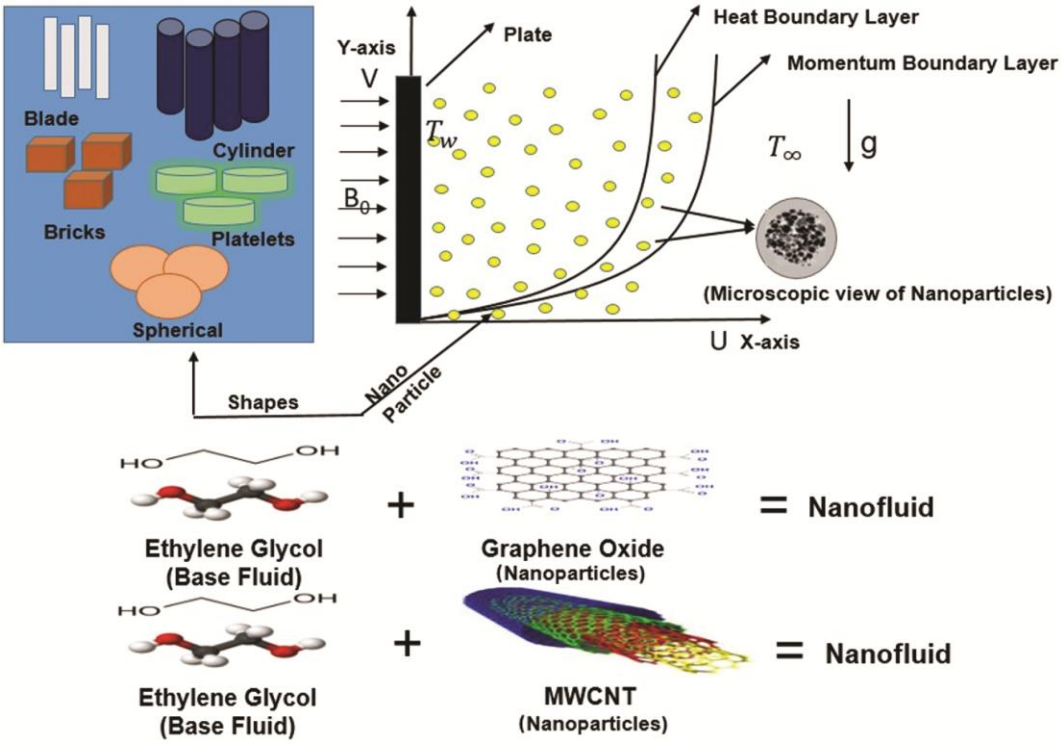

Fig. 1 — Geometrical demonstration of the problem

Note that $t=0$ is the initial temperature and T_w is temperature of the plate at time t. The temperature and velocity fields are shown below: The construction of mathematical governing equations summarized by Boussinesq's approximations.

$$\vec{V}=u\left(x,t\right)\hat{i}, \quad \text{... (1)}$$

$$T=T\left(x,t\right) \quad \text{... (2)}$$

the Casson fluids constructive equations are:

$$\nabla.\vec{V}=0, \quad \text{... (3)}$$

$$\rho\frac{d\vec{V}}{dt}=div(\tau_{ij})+\rho\vec{\mathrm{b}}+\left(\bar{J}\times\bar{B}\right) \quad \text{... (4)}$$

Where, ρ is density of the fluid, $\frac{d}{dt}$ is substantial time derivative, $\vec{b}$ is body force and τ_{ij} is Cauchy stress tensor represented as:

The rheological equation for unstable Casson fluid flow is stated by Casson (1959) and is given as follows:

$$\tau_{ij}=\begin{cases}2e_{ij}\left(\mu_{\gamma}+\dfrac{p_y}{\sqrt{2\pi_1}}\right); & \pi_1>\pi_c\\ 2e_{ij}\left(\mu_{\gamma}+\dfrac{p_y}{\sqrt{2\pi_c}}\right); & \pi_1<\pi_c\end{cases} \quad \text{... (5)}$$

In Eq. (5) , μ represent dynamic viscosity, μ_{γ} denotes the plastic dynamic viscosity of the non-Newtonian fluid flow $\left(\mu_{\gamma}=\rho\nu\right)$ and p_y is yield stress of the fluid, π_c denotes the critical value of the number π_1, $\pi_1=e_{ij}e_{ij}$ where e_{ij} is the component of the non-Newtonian fluid deformation rate and also the component deformation rate of (i, j)[th] can be written as:

$$e_{ij}=-PI+\mu A_1 \quad \text{... (6)}$$

Where P is indeterminate pressure, I is identity tensor, μ is dynamic viscosity and A_1 is Rivlin-Erickson tensor of first kind,

$$div\left(\tau_{ij}\right)=\left(\mu_{\gamma}+\frac{p_y}{\sqrt{2\pi_1}}\right)\frac{\partial^2u}{\partial y^2} \quad \text{... (7)}$$

$\rho\vec{b}$ indicates the body force which include Lorentz and bouncy forces, defined as:

$$\rho\vec{b}=\rho g\gamma\left(T-T_{\infty}\right) \quad \text{... (8)}$$

$$\bar{J}\times\bar{B}=-\sigma B_0^2u \quad \text{... (9)}$$

Using Eqs. (7), (8) and (9), it can be expressed Eqs. (3) and (4) in Cartesian form of nanofluids. Thus, converting the equations to a fractional model such as[1,41]:

$$\rho_{nf}D_t^{\alpha}u=\left(\mu_B\right)_{nf}\left(1+\frac{1}{\beta}\right)\frac{\partial^2u}{\partial x^2}+\left(\rho\gamma\right)_{nf}g\left(T-T_{\infty}\right)-\sigma_{nf}B_0^2u \quad \text{... (10)}$$

$$\left(\rho C_p\right)_{nf}D_t^{\alpha}T=k_{nf}\frac{\partial^2T}{\partial x^2} \quad \text{...(11)}$$

With the following appropriate initial and boundary conditions:

$$\left.\begin{array}{ll}t\le 0: u=0, T=T_{\infty} & \forall x>0,\\ t>0: u=U, T=T_w & at\ x=0,\\ u\to 0, T\to T_{\infty} & as\ x\to\infty\end{array}\right\} \quad \text{... (12)}$$

Where β is the material parameter of Casson fluid, ϕ is the volume fraction, g is acceleration constant, σ is the electrical conductivity and γ symbolizes volumetric coefficient of Ethylene glycol nanoparticles.

To construct the dimensionless modal equations, introducing the suitable non-dimensional variables can be suggested as

$$u^*=\frac{u}{U},\qquad x^*=\frac{U}{\vartheta_f}x,\qquad \tau^*=\frac{U^2}{\vartheta_f}t,\qquad \theta=\frac{T-T_{\infty}}{T_w-T_{\infty}} \quad \text{... (13)}$$

using the above dimensionless variables and drop the star note, the governing Eqs. (10), (11) and following conditions can be written as:

$$D_{\tau}^{\alpha}u=a_6\left(1+\frac{1}{\beta}\right)\frac{\partial^2u}{\partial x^2}+a_8Gr\theta-a_{10}M\,u \quad \text{... (14)}$$

And

$$D_{\tau}^{\alpha}\theta=\frac{a_3}{pr}\frac{\partial^2\theta}{\partial x^2} \quad \text{... (15)}$$

With the corresponding initial and boundary conditions

$$\left.\begin{array}{lll} u(x,0)=0, & \theta(x,0)=0; & x>0 \\ u(0,\tau)=1, & \theta(0,\tau)=1; & x=0 \\ u(x,\tau)\to 0, & \theta(x,\tau)\to 0; & x\to\infty, t>0 \end{array}\right\} \quad \text{... (16)}$$

Where

$$\Pr=\frac{\mu C_p}{k}, Gr=\frac{g\gamma_f \vartheta_f (T_w-T_\infty)}{U^3}, \beta=\frac{\mu_B\sqrt{2\pi_c}}{p_y}, M=\frac{\sigma_f B_0^2 \vartheta_f}{\rho_f U^2}$$

are the Prandtl number, the Grashof number, the Casson parameter and the magnetic field parameter, respectively.

Letting parameters are,

$$a_1=\frac{k_p+2k_f+2\phi(k_p-k_f)}{k_p+2k_f-\phi(k_p-k_f)}, a_2=(1-\phi)+\phi\frac{(\rho C_p)_p}{(\rho C_p)_f},$$

$$a_3=\frac{a_1}{a_2}, a_4=(1-\phi)+\phi\frac{\rho_p}{\rho_f}, \quad a_5=(1-\phi)^{2.5}, a_6=\frac{1}{a_4 a_5},$$

$$a_7=(1-\phi)+\phi\frac{(\rho\gamma)_p}{(\rho\gamma)_f}, a_8=\frac{a_7}{a_4},$$

$$a_9=\left[1+\frac{3\phi\left(\frac{\sigma_p}{\sigma_f}-1\right)}{\left(\frac{\sigma_p}{\sigma_f}+2\right)-\phi\left(\frac{\sigma_p}{\sigma_f}-1\right)}\right], \quad a_{10}=\frac{a_9}{a_4}, B_1=a_{10}M,$$

$$B_2=a_6\xi pr, B_3=\frac{a_3B_1}{B_2-a_3}, B_4=\frac{-Gra_3a_8}{B_2-a_3}, B_5=a_6\xi,$$

$$B_6=\frac{B_1}{B_5}, B_7=\frac{B_3}{B_5}+B_6.$$

Analytical solution

The main aim of this session is to derive exact solutions of the Caputo fractional model. In the current investigation, by using the coupled Fourier Sine and Laplace transforms, presented the analytic solutions for partial differential equations of fractional order. The amalgamation between the FSTs and Laplace transform is reported in the literature in the following investigations[1] and can also be found in many papers. The advantage of this method in the present research is it permits the obtaining of the linear fractional differential equations.

Solution of temperature field

Let us considered Eq. (15) represents the heat equation, subjected to the initial and boundary conditions in Eq. (16). Using Fourier sine transform formula, we have $F_s\left[D_\tau^\alpha\theta(x,\tau)\right]=D_\tau^\alpha\theta(q,\tau)$ and $F_s\left[\frac{\partial^2\theta(x,\tau)}{\partial x^2}\right]=\frac{a_3}{Pr}\left[q-q^2\theta(q,\tau)\right]$, Here F_s represents the Fourier sine transformation and q is the Fourier sine variable. Apply the Fourier sine transformation to the previous equation, we get the following relationship

$$\left(s^\alpha+\frac{a_3q^2}{Pr}\right)\bar{\theta}(q,s)=\frac{a_3q}{Pr}\frac{1}{s},$$
$$D_\tau^\alpha\theta(q,\tau)=\frac{a_3}{Pr}\left[q-q^2\theta(q,\tau)\right] \quad \text{... (17)}$$

The next step is Laplace transformation, Applying Laplace transformation on both sides of Eq. (17) and further rearrangement of the equations, we obtain the following relation

$$s^\alpha\bar{\theta}(q,s)-s^{\alpha-1}\theta(q,0)=\frac{a_3q}{Pr}\frac{1}{s}-\frac{a_3q^2}{Pr}\bar{\theta}(q,s)$$

$$s^\alpha\bar{\theta}(q,s)=\frac{a_3q}{Pr}\frac{1}{s}-\frac{a_3q^2}{Pr}\bar{\theta}(q,s)$$

$$\bar{\theta}(q,s)=\frac{a_3q}{s\,Pr\left(s^\alpha+\frac{a_3q^2}{Pr}\right)}$$

$$\bar{\theta}(q,s)=\frac{1}{q}\left\{\frac{1}{s}-\frac{s^{\alpha-1}}{s^\alpha+\frac{a_3q^2}{Pr}}\right\} \quad \text{... (18)}$$

And then applying the inverse Laplace transformation, we get

$$\theta(q,\tau)=\frac{1}{q}\left[1-E_\alpha\left(\frac{-a_3q^2}{Pr}\tau^\alpha\right)\right] \quad \text{... (19)}$$

Succeeding the procedure in[1], at last apply the inverse Fourier sine transformation to Eq. (19). By using the formula of the inverse Fourier sine transform, we get the following solution for temperature field:

$$\theta(x,\tau)=\frac{2}{\pi}\int_0^\infty\frac{1}{q}\left\{1-E_\alpha\left(\frac{-a_3q^2}{Pr}\tau^\alpha\right)\right\}\sin qx\,dq,$$

$$\theta(x,\tau)=\frac{2}{\pi}\left[\int_0^\infty \frac{1}{q}\sin qx\,dq-\int_0^\infty \frac{1}{q}E_\alpha\left(\frac{-a_3q^2}{Pr}\tau^\alpha\right)\sin qx\,dq\right]$$

$$\theta(x,\tau)=1-\frac{2}{\pi}\int_0^\infty E_\alpha\left(\frac{-a_3q^2}{Pr}\tau^\alpha\right)\frac{\sin qx}{q}\,dq \quad \text{... (20)}$$

Limiting Case: by making $(\alpha\to 1)$

$$s\bar{\theta}(q,s)-\theta(q,0)=\frac{a_3q}{Pr}\frac{1}{s}-\frac{a_3q^2}{Pr}\bar{\theta}(q,s)$$

$$s\bar{\theta}(q,s)=\frac{a_3q}{Pr}\frac{1}{s}-\frac{a_3q^2}{Pr}\bar{\theta}(q,s)$$

$$\bar{\theta}(q,s)=\frac{a_3q}{s\,Pr\left(s+\frac{a_3q^2}{Pr}\right)}$$

$$\bar{\theta}(q,s)=\frac{1}{q}\left(\frac{1}{s}-\frac{1}{s+\frac{a_3q^2}{Pr}}\right) \quad \text{... (21)}$$

Applying inverse Laplace transform, we get

$$\theta(q,\tau)=\frac{1}{q}\left\{1-\exp\left(-\frac{a_3q^2}{Pr}\tau\right)\right\} \quad \text{... (22)}$$

Applying inverse Fourier sine transform for Eq. 22, we get

$$\theta(x,\tau)=\frac{2}{\pi}\int_0^\infty\frac{1}{q}\left\{1-\exp\left(-\frac{a_3q^2}{Pr}\tau\right)\right\}\sin qx\,dq$$

$$\theta(x,\tau)=\frac{2}{\pi}\left\{\int_0^\infty\frac{\sin qx}{q}dq-\int_0^\infty\frac{1}{q}\exp\left(-\frac{a_3q^2}{Pr}\tau\right)\sin qx\,dq\right\}$$

$$\theta(x,\tau)=1-\frac{2}{\pi}\int_0^\infty\exp\left(-\frac{a_3q^2}{Pr}\tau\right)\frac{\sin qx}{q}\,dq$$

$$\theta(x,\tau)=1-erf\left(\frac{x\sqrt{Pr}}{2\sqrt{a_3\tau}}\right)=erfc\left(\frac{x\sqrt{Pr}}{2\sqrt{a_3\tau}}\right) \quad \text{... (23)}$$

Solution of velocity field

To Eq. (14) we apply the Fourier sine transformation on both sides we get,

$$D_\tau^\alpha u(q,\tau)=a_6\left(1+\frac{1}{\beta}\right)\left\{q\,u(0,\tau)-q^2u(q,\tau)\right\}+a_8Gr\,\theta(q,\tau)-a_{10}M\,u(q,\tau)$$

We take that $\xi=\left(1+\frac{1}{\beta}\right)$,

$$D_\tau^\alpha u(q,\tau)=a_6\xi q-a_6\xi q^2u(q,\tau)+a_8Gr\,\theta(q,\tau)-a_{10}M\,u(q,\tau) \quad \text{... (24)}$$

Next step, applying the Laplace transform on both sides of Eq. (24)we get,

$$s^\alpha\bar{u}(q,s)-s^{\alpha-1}u(q,0)=a_6\xi q\frac{1}{s}-a_6\xi q^2\bar{u}(q,s)+a_8\bar{\theta}(q,s)Gr-a_{10}M\,\bar{u}(q,s)$$

$$s^\alpha\bar{u}(q,s)=a_6\xi q\frac{1}{s}-a_6\xi q^2\bar{u}(q,s)+\bar{\theta}(q,s)a_8Gr-a_{10}M\,\bar{u}(q,s)$$

$$\bar{u}(q,s)=\frac{a_6\xi q}{s\left(s^\alpha+a_6\xi q^2+a_{10}M\right)}+\frac{a_8Gr\,\bar{\theta}(q,s)}{\left(s^\alpha+a_6\xi q^2+a_{10}M\right)} \quad \text{... (25)}$$

Next step, applying the inverse Laplace transform in Eq. (25), to make the simplification easy we consider two Laplace transform functions as

$$\bar{a}(q,s)=\frac{a_6\xi q}{s\left(s^\alpha+a_6\xi q^2+a_{10}M\right)} \quad \text{... (26)}$$

$$\bar{b}(q,s)=\frac{Gra_3a_8q}{s\,Pr\left(s^\alpha+a_6\xi q^2+a_{10}M\right)\left(s^\alpha+\frac{a_3q^2}{Pr}\right)} \quad \text{... (27)}$$

Inverting the function $\bar{b}$ by applying the inverse Laplace transform, we obtain the following relation

$$\bar{b}(q,s)=\frac{Gra_3a_8}{Pr\,q\left(a_6\xi-\frac{a_3}{Pr}+\frac{a_{10}M}{q^2}\right)}\left\{\frac{s^{\alpha-(1+\alpha)}}{\left(s^\alpha+\frac{a_3q^2}{Pr}\right)}-\frac{s^{\alpha-(1+\alpha)}}{\left(s^\alpha+a_6\xi q^2+a_{10}M\right)}\right\}$$

$$\bar{b}(q,\tau)=\frac{Gra_3a_8\tau^\alpha}{Pr\,q\left(a_6\xi-\frac{a_4}{Pr}+\frac{a_{10}M}{q^2}\right)}\left\{E_{\alpha,\beta}\left(-\frac{a_3q^2}{Pr}\tau^\alpha\right)-E_{\alpha,\beta}\left(-\left(a_6q^2\xi+a_{10}M\right)\tau^\alpha\right)\right\} \quad \text{... (28)}$$

By applying the inverse Fourier sine transform to both the sides of Eq. (28), we get

$$b(x,\tau)=\frac{2Gra_3a_8}{k}\int_0^\infty\frac{\sin qx}{q}\tau^\alpha\left\{E_{\alpha,\beta}\left(-\frac{a_3q^2}{Pr}\tau^\alpha\right)-E_{\alpha,\beta}\left(-\left(a_6q^2\xi+a_{10}M\right)\tau^\alpha\right)\right\}dq \quad \text{... (29)}$$

Where $\beta=1+\alpha$ and $k=Pr\,\pi\left(a_6\xi-\frac{a_3}{Pr}+\frac{a_{10}M}{q^2}\right)$.

We repeat the same procedure for solving the function $\bar{a}$.Before applying inverse Laplace transform rewrite the function $\bar{a}$ is

$$\bar{a}(q,s)=\frac{a_6\xi}{q\left(a_6\xi+\frac{a_{10}M}{q^2}\right)}\left(\frac{1}{s}-\frac{s^{\alpha-1}}{s^{\alpha}+a_6\xi q^2+a_{10}M}\right) \quad \text{... (30)}$$

Applying the inverse Laplace transform we get,

$$\bar{a}(q,\tau)=\frac{a_6\xi}{q\left(a_6\xi+\frac{a_{10}M}{q^2}\right)}\left\{1-E_{\alpha}\left(-\left(a_6q^2\xi+a_{10}M\right)\tau^{\alpha}\right)\right\} \quad \text{... (31)}$$

Taking inverse Fourier sine transform on the both sides of Eq. (31)

$$a(x,\tau)=\frac{2}{\pi}\int_0^{\infty}\frac{\sin qx}{q}\left\{\frac{a_6\xi}{\left(a_6\xi+\frac{a_{10}M}{q^2}\right)}\left[1-E_{\alpha}\left(-\left(a_6q^2\xi+a_{10}M\right)\tau^{\alpha}\right)\right]\right\}dq \quad \text{... (32)}$$

Finally, adding Eqns. (29) and (32) is the analytical solution of velocity Eq. (13). That is

$$u(x,\tau)=a(x,\tau)+b(x,\tau) \quad \text{... (33)}$$

Limiting Case: by making $(\alpha\to 1)$

Take $\alpha=1$ in Eq. (25), we get

$$\bar{u}(q,s)=\frac{a_6\xi q}{s\left(s+a_6\xi q^2+a_{10}M\right)}+\frac{a_8Gr\bar{\theta}(q,s)}{\left(s+a_6\xi q^2+a_{10}M\right)} \quad \text{... (34)}$$

Applying the inverse Laplace transform in Eq. (34),

$$u(q,\tau)=a_6\xi q\,L^{-1}\left[\frac{1}{s\left(s+a_6\xi q^2+a_{10}M\right)}\right]+a_8Gr\,L^{-1}\left[\frac{\bar{\theta}(q,s)}{\left(s+a_6\xi q^2+a_{10}M\right)}\right] \quad \text{... (35)}$$

By simplification we get,

$$L^{-1}\left[\frac{1}{s\left(s+a_6\xi q^2+a_{10}M\right)}\right]=\frac{a_6\xi}{q^2\left(a_6\xi+\frac{a_{10}M}{q^2}\right)}\left(1-e^{-\left(a_6\xi q^2+a_{10}M\right)\tau}\right) \quad \text{... (36)}$$

$$L^{-1}\left[\frac{\bar{\theta}(q,s)}{\left(s+a_6\xi q^2+a_{10}M\right)}\right]=\frac{1}{q^3\left(a_6\xi-\frac{a_3}{Pr}+\frac{a_{10}M}{q^2}\right)}\left(1-e^{-\frac{a_3q^2}{Pr}\tau}\right)-\frac{a_3}{Pr\,q^3\left(a_6\xi-\frac{a_3}{Pr}+\frac{a_{10}M}{q^2}\right)\left(a_6\xi+\frac{a_{10}M}{q^2}\right)}\left(1-e^{-\left(a_6\xi q^2+a_{10}M\right)\tau}\right) \quad \text{... (37)}$$

Substitute Eqns. (36) and (37) in Eq. (35), we get,

$$u(q,\tau)=\frac{a_6\xi}{q\left(a_6\xi+\frac{a_{10}M}{q^2}\right)}\left(1-e^{-\left(a_6\xi q^2+a_{10}M\right)\tau}\right)+\frac{Gr\,a_8}{q^3\left(a_6\xi-\frac{a_3}{Pr}+\frac{a_{10}M}{q^2}\right)}\left(1-e^{-\frac{a_3q^2}{Pr}\tau}\right)-\frac{Gra_3a_8}{Pr\,q^3\left(a_6\xi-\frac{a_3}{Pr}+\frac{a_{10}M}{q^2}\right)\left(a_6\xi+\frac{a_{10}M}{q^2}\right)}\left(1-e^{-\left(a_6\xi q^2+a_{10}M\right)\tau}\right) \quad \text{... (38)}$$

Applying inverse Fourier sine transform, we get

$$u(x,\tau)=\frac{2}{\pi}\int_0^{\infty}\left[\frac{a_6\xi}{q\left(a_6\xi+\frac{a_{10}M}{q^2}\right)}\left(1-e^{-\left(a_6\xi q^2+a_{10}M\right)\tau}\right)+\frac{Gra_8}{q^3\left(a_6\xi-\frac{a_3}{Pr}+\frac{a_{10}M}{q^2}\right)}\left(1-e^{-\frac{a_3q^2}{Pr}\tau}\right)-\frac{Gra_3a_8}{Pr\,q^3\left(a_6\xi-\frac{a_3}{Pr}+\frac{a_{10}M}{q^2}\right)\left(a_6\xi+\frac{a_{10}M}{q^2}\right)}\left(1-e^{-\left(a_6\xi q^2+a_{10}M\right)\tau}\right)\right]\sin qx\,dq$$

$$u(x,\tau)=\frac{2}{\pi}\int_0^{\infty}\left[\frac{\frac{a_6\xi}{\left(a_6\xi+\frac{a_{10}M}{q^2}\right)}\left(1-e^{-\left(a_6\xi q^2+a_{10}M\right)\tau}\right)+\frac{Gra_8}{q^2\left(a_6\xi-\frac{a_3}{Pr}+\frac{a_{10}M}{q^2}\right)}\left(1-e^{-\frac{a_3q^2}{Pr}\tau}\right)}{-\frac{Gra_3a_8}{Pr\,q^2\left(a_6\xi-\frac{a_3}{Pr}+\frac{a_{10}M}{q^2}\right)\left(a_6\xi+\frac{a_{10}M}{q^2}\right)}\left(1-e^{-\left(a_6\xi q^2+a_{10}M\right)\tau}\right)}\right]\frac{\sin qx}{q}\,dq$$

$$u(x,\tau)=\left(1+\frac{B_4}{B_3}\right)\frac{1}{2}\left[e^{x\sqrt{B_5}}erfc\left(\frac{x}{2\sqrt{B_5\tau}}+\sqrt{B_5B_6\tau}\right)+e^{-x\sqrt{B_5}}erfc\left(\frac{x}{2\sqrt{B_5\tau}}-\sqrt{B_5B_6\tau}\right)\right]-\frac{B_4}{B_3}\frac{e^{B_5\tau}}{2}\left[e^{x\sqrt{B_5}}erfc\left(\frac{x}{2\sqrt{B_5\tau}}+\sqrt{B_5B_7\tau}\right)+e^{-x\sqrt{B_5}}erfc\left(\frac{x}{2\sqrt{B_5\tau}}-\sqrt{B_5B_7\tau}\right)\right]-\frac{B_4}{B_3}erfc\left(\frac{x\sqrt{Pr}}{2\sqrt{a_3\tau}}\right)+\frac{B_4}{B_3}\frac{e^{B_3\tau}}{2}\left[e^{x\sqrt{\frac{B_3Pr}{a_3}}}erfc\left(\frac{x\sqrt{Pr}}{2\sqrt{a_3\tau}}+\sqrt{B_3\tau}\right)+e^{-x\sqrt{\frac{B_3Pr}{a_3}}}erfc\left(\frac{x\sqrt{Pr}}{2\sqrt{a_3\tau}}-\sqrt{B_3\tau}\right)\right] \quad \text{... (39)}$$

Expressions of Nussult number and skin friction

The key engineering factors are given by:

$$Nu=-\left.\frac{\partial\theta}{\partial x}\right|_{x=0} \quad \text{... (40)}$$

$$C_f=-\left.\frac{\partial u}{\partial x}\right|_{x=0} \quad \text{... (41)}$$

From Eqns. (20) and (40), we evaluate the Nussult number as follows:

$$Nu=\sqrt{\frac{Pr}{a_3}}L^{-1}\left[s^{\frac{\alpha}{2}-1}\right]=\sqrt{\frac{Pr}{a_3}}\frac{t^{-\frac{\alpha}{2}}}{\Gamma\left(1-\frac{\alpha}{2}\right)} \quad \text{... (42)}$$

From Eqns. (33) and (41), we derived the skin-friction coefficient as follows:

$$C_f=\frac{1}{\sqrt{a_6\xi}}L^{-1}\left[\frac{\sqrt{s^{\alpha-1}}}{s}\right]-\frac{B_4}{\sqrt{a_6\xi}}L^{-1}\left[\frac{\sqrt{s^{\alpha}+B_1}}{s\left(s^{\alpha}-B_3\right)}\right]+B_4\sqrt{\frac{Pr}{a_3}}L^{-1}\left[\frac{\sqrt{s^{\alpha}}}{s\left(s^{\alpha}-B_3\right)}\right] \quad \text{... (43)}$$

$$C_f = \frac{1}{\sqrt{a_6\xi}}\left[\frac{t^{-\frac{\alpha}{2}}}{\Gamma\left(-\frac{\alpha}{2}+1\right)} - \sum_{k=1}^{\infty}\frac{(2k-2)!(-1)^k B_1^k t^{\alpha\left(k-\frac{1}{2}\right)}}{2^{2k-1}k!(k-1)!\Gamma\left(\alpha\left(k-\frac{1}{2}\right)+1\right)}\right]$$
$$-\frac{B_4}{\sqrt{a_6\xi}\Gamma\left(-\frac{\alpha}{2}+1\right)}\int_0^t u^{\alpha-1}E_{\alpha,\alpha}\left(B_3u^{\alpha}\right)(t-u)^{-\frac{\alpha}{2}}du$$
$$+\frac{B_4}{\sqrt{a_6\xi}}\sum_{k=1}^{\infty}\frac{(2k-2)!(-1)^k B_1^k}{2^{2k-1}k!(k-1)!\Gamma\left(\alpha\left(k-\frac{1}{2}\right)+1\right)}\int_0^t u^{\alpha-1}E_{\alpha,\alpha}\left(B_3u^{\alpha}\right)(t-u)^{\alpha\left(k-\frac{1}{2}\right)}du$$
$$+B_4\sqrt{\frac{Pr}{a_3}}\frac{1}{\Gamma\left(-\frac{\alpha}{2}+1\right)}\int_0^t u^{\alpha-1}E_{\alpha,\alpha}\left(B_3u^{\alpha}\right)(t-u)^{-\frac{\alpha}{2}}du \quad \text{... (44)}$$

Discussions on graphical and tabular results

The fluid with unsteady, convective, incompressible MHD flow of non-Newtonian Casson fluid consisting EG-GO and EG-MWCNT's nanoparticles through a vertical flat infinite plate is considered. Caputo fractional derivative is used to obtain the exact analytical solutions of dimensionless energy and momentum equations by using the combination of Fourier sine and Laplace transformations. The fascinating behaviour of different physical parameters on temperature and velocity of investigated problem, plotted via graphical representations by using the software MATLAB. The impact of the physical parameters such as α, Pr, Gr, ϕ, β, M which are fractional parameter, Prandtl number, thermal Grashof number, volume fraction, Casson parameter and magnetic field parameter, respectively, on temperature and fluid transport are investigated besides that also examined the dynamics of the physical results when $\tau = 0.5$ and $\tau = 1.5$. Explained the influence of the Caputo fractional derivative model used in this problem. In Fig. 1 the geometry of the current problem is displayed. The thermophysical properties of the host fluid Ethylene glycol(EG) and the nanoparticles Graphene oxide(GO), Multiwall Carbon nanotubes (MWCNT's) are listed in Table 1 and Table 2, respectively. Table 3 indicates the various shapes of nano particles. Calculated values of Nussult number and Skin-friction presented in Table 4 and Table 5, respectively.

Temperature profiles

We begin the analysis with heat Eq. (15), which is having the solution given in Eq. (20). Temperature profiles are plotted to understand a comparison between EG-GO and EG-MWCNT's nanofluids. The effect of Caputo fractional parameter α on thermal distribution is shown in Fig. 2 and Prandtl number is fixed at $\Pr = 6.2$. We observe that in Fig. 2(a), considered time $\tau = 0.5$, when the fractional order derivative raises the tendency of fractional thermal equation is raising as well as decreases. Which means when the time is less than 1, the derivative of Caputo fractional operator has simulation diffusion effect in the process. In Fig. 2(b) consider time $\tau = 1.5$, when the order increases as well as the heat diffusion is also increases. The arrow represents the direction of the

Table 1 — Thermophysical properties of nanofluids[49]

Properties	Nanofluid
Density	$\rho_{nf} = (1-\phi)\rho_f + \phi\rho_p$
Heat capacity	$(\rho C_p)_{nf} = (1-\phi)(\rho C_p)_f + \phi(\rho C_p)_p$
Volumetric coefficient	$(\rho\gamma)_{nf} = (1-\phi)(\rho\gamma)_f + \phi(\rho\gamma)_p$
Dynamic viscosity (Brinkman Model)	$\mu_{nf} = \frac{\mu_f}{(1-\phi)^{2.5}}$
Thermal conductivity (Maxwell Model)	$\frac{k_{nf}}{k_f} = \left[\frac{k_p + (n-1)k_f + (n-1)\phi(k_p - k_f)}{k_p + (n-1)k_f - \phi(k_p - k_f)}\right]$
Electrical conductivity	$\frac{\sigma_{nf}}{\sigma_f} = \left[1 + \frac{3\phi\left(\frac{\sigma_p}{\sigma_f} - 1\right)}{\left(\frac{\sigma_p}{\sigma_f} + 2\right) - \phi\left(\frac{\sigma_p}{\sigma_f} - 1\right)}\right]$

Table 2 — Thermophysical properties of host fluid and nanoparticles[49,50]

Thermo-Physical Properties	Host fluid (Ethylene Glycol)	Nanoparticles	
		Graphene Oxide	MWCNT's
$\rho\left(Kg.\mathrm{m}^{-3}\right)$	1114	1800	1600
$C_p\left(J\,Kg^{-1}K^{-1}\right)$	3630	717	796
$K\left(W\,m^{-1}K^{-1}\right)$	0.252	5000	3000
$\sigma\left(S\,m^{-1}\right)$	5.5×10^{-6}	6.30×10^{7}	10^{7}
$\gamma\times10^{-5}\left(k^{-1}\right)$	57	2.84×10^{-4}	44

dynamical behaviour of fluid temperature. In Fig. 3 it is displayed that the impact of the volume fraction ϕ at distinct times $\tau = 0.5$ and 1.5. With an increase in the values of ϕ then temperature also increases because the thermal conductivity of nanofluids rises by raising the volume fraction ϕ. In this paper, weconsider five distinct shapes (blade, platelet, cylindrical, brick and spherical) of nano sized particles. Fig. 4 represents the variations of temperature distribution for different shapes of nano particles. We observe that blade shaped nanoparticles gives the effective results for temperature distribution. A comparison between temperature profiles of pure base fluid Ethylene glycol, nanofluids EG-GO and EG-MWCNT's are drawn in Fig. 5. It is observed that EG-MWCNT's nanofluid is more effective than EG-GO nanofluid.

Table 3 — Values of n corresponding to different shapes of nanoparticles[29]

Shape		n
Blade		8.3
Platelet	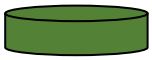	5.7
Cylinder		4.9
Brick		3.7
Spherical	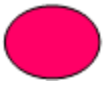	3

Velocity profiles

This section we begin with the analysis of velocity Eq. (14), which is having the solution given in Eq. (33) by plotting graphs for various values of fractional derivative parameter at two various times $\tau = 0.5$ and $\tau = 1.5$ while other parameters such as the Casson Parameter, volume fraction, Prandtl number and

Table 4 — Numerical values of Nussult number

Pr	t	α	ϕ	Nu	
				EG-GO	EG-MWCNT
6.2	0.5	0.65	0.03	2.204720922981094	2.204588711516918
9	-	-	-	2.656311690261258	2.656152398055966
12	-	-	-	3.067244538847775	3.067060604052565
-	1.0	-	-	1.760025155182551	1.759919610984042
-	1.5	-	-	1.542727481122530	1.542634967708711
-	-	0.80	-	2.088871112927400	2.088745848679470
-	-	0.95	-	1.938795029298545	1.938678764728781
-	-	-	0.04	2.165363531108934	2.165188987268812
-	-	-	0.05	2.126905912865792	2.126689863754161

Table 5 — Numerical analysis of Skin-friction coefficient

Pr	t	α	β	Gr	ϕ	M	C_f	
							EG-GO	EG-MWCNT
6.2	0.5	0.65	0.5	5	0.03	0.5	-0.844075806784696	-0.859203405972172
9	-	-	-	-	-	-	-0.858722571828727	-0.873092122255381
12	-	-	-	-	-	-	-0.865894179074936	-0.879083677512725
-	1.0	-	-	-	-	-	-0.885914535676654	-0.901244883493232
-	1.5	-	-	-	-	-	-0.892711217503574	-0.907537066607193
-	-	0.80	-	-	-	-	-0.881816568152140	-0.896659283412883
-	-	0.95	-	-	-	-	-0.927822719984897	-0.943913258287680
-	-	-	1.0	-	-	-	-1.484403124617359	-1.507738895840512
-	-	-	1.5	-	-	-	-1.902582135273361	-1.926627988190905
-	-	-	-	6	-	-	-1.143466241666967	-1.160964031681538
-	-	-	-	7	-	-	-1.441706529315939	-1.463241536592930
-	-	-	-	-	0.04	-	-0.805073594047506	-0.824918215344650
-	-	-	-	-	0.05	-	-0.766433032424698	-0.791377032078322
-	-	-	-	-	-	1	-0.750042510958862	-0.764451747066493
-	-	-	-	-	-	1.5	-0.670735082023437	-0.685712912550201

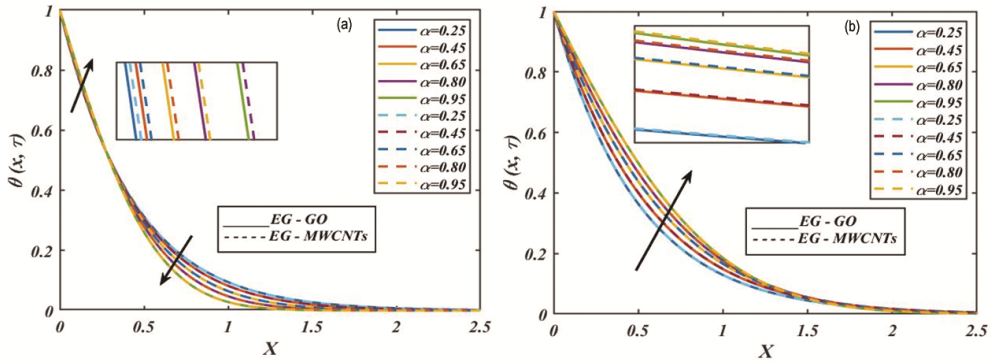

Fig. 2 — Graphical representation of the temperature field with distinct values of α the fractional parameter (a) $\tau = 0.5$ and (b) $\tau = 1.5$ for $Pr = 6.2$, $n = 3$ and $\phi = 0.05$

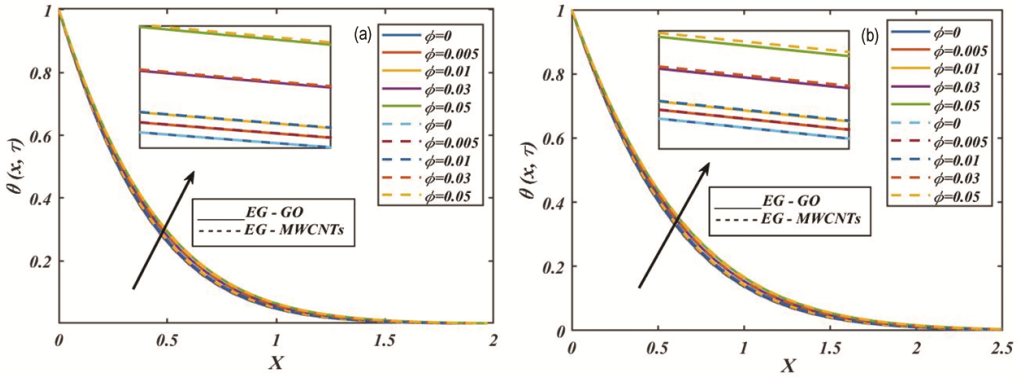

Fig. 3 — Graphical representation of the temperature field with different values of volume fraction ϕ (a) $\tau = 0.5$ and (b) $\tau = 1.5$ for $\alpha = 0.65$, $n = 3$ and $Pr = 6.2$

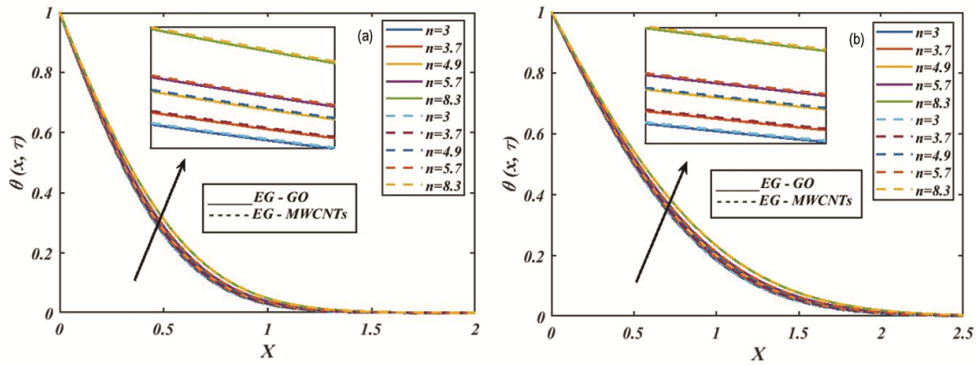

Fig. 4 — Graphical representation of the temperature fieldwith different shapes of nanoparticles (a) $\tau = 0.5$ and (b) $\tau = 1.5$ for $\alpha = 0.95$, $\phi = 0.05$ and $Pr = 6.2$

Grashof number, Magnetic field parameter being fixed to particular values. Velocity profiles are plotted to understand a comparison between EG-GO and EG-MWCNT's nanofluids. The velocity distribution behaviour for fractional operator is presented in Fig. 6. The influence of Caputo fractional operator α can be useful in many physical situations to get an accurate result on fluid velocity by varying α. It is observed that when time $\tau = 0.5$ in Fig. 6(a), when Caputo order derivative operator rises, then the velocity falls. It can also be noticed that a reverse phenomena exhibited in Fig. 6(b) when $\tau = 1.5$ such as, the Caputo order derivative parameter increases the velocity rises.

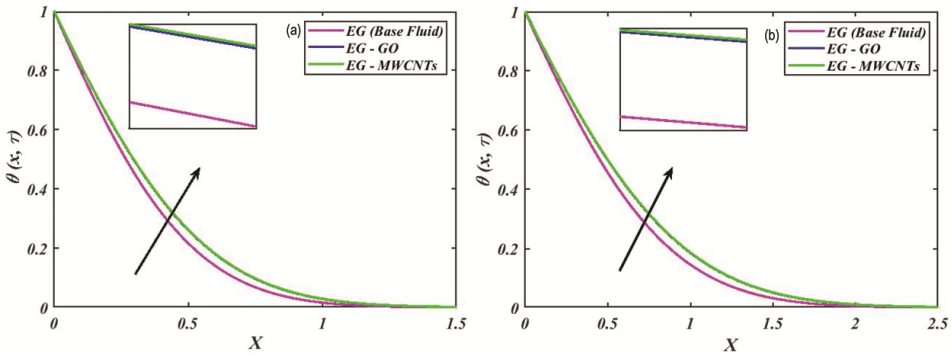

Fig. 5 — Graphical representation of the fluid temperature with various nanoparticles (a) $\tau = 0.5$ and (b) $\tau = 1.5$ for $\alpha = 0.95$, $\phi = 0.05$, $n = 3$ and $Pr = 6.2$.

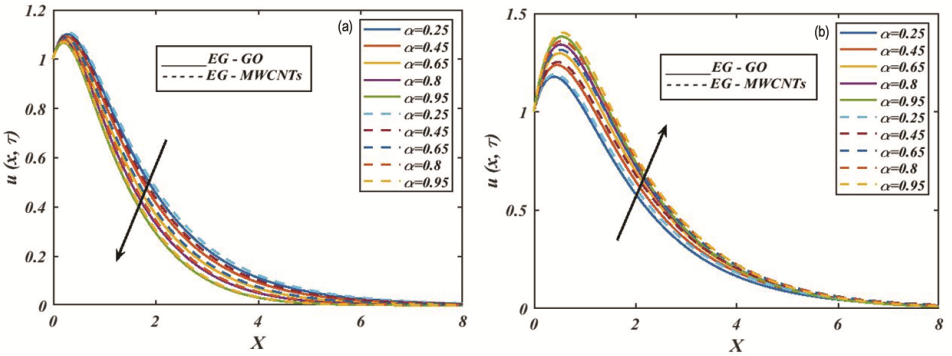

Fig. 6 — Graphical representation of the velocity with various values of fractional parameter α (a) $\tau = 0.5$ and (b) $\tau = 1.5$, for $\beta = 0.5$, $\phi = 0.05$, $n = 3, Pr = 6.2$, $M = 0.5$ and $Gr = 5$

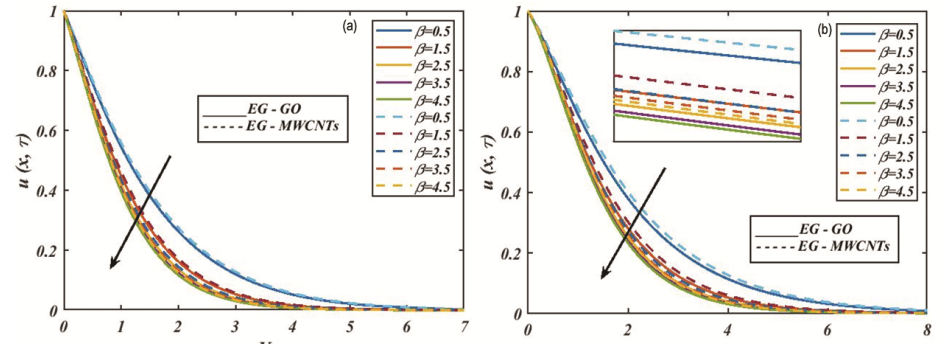

Fig. 7 — Graphical representation of the velocity with various values of β (a) $\tau = 0.5$ and (b) $\tau = 1.5$ for $\alpha = 0.65$, $\phi = 0.05$, $Pr = 6.2$, $n = 3, M = 0.5$ and $Gr = 5$

Fig. 7 shows the impact of Casson parameter β in two different time values. We observe that, when β raises, velocity reduces. The physical reason is illustrated that when increasing the Casson fluid parameter the viscosity of velocity boundary layer turns down. While the Grashof number represents the ratio between the buoyancy forces due to spatial variation in fluid density (caused by temperature differences) to the restraining force due to the viscosity of the fluid. The real-world situations mean the natural convection plays a vital role in the progress of flow that states Gr is the most significant physical parameter.

In Fig. 8, we observed the impact of thermal Grashof number Gr on velocity distribution. We observed that when thermal Gr raises (for cooling

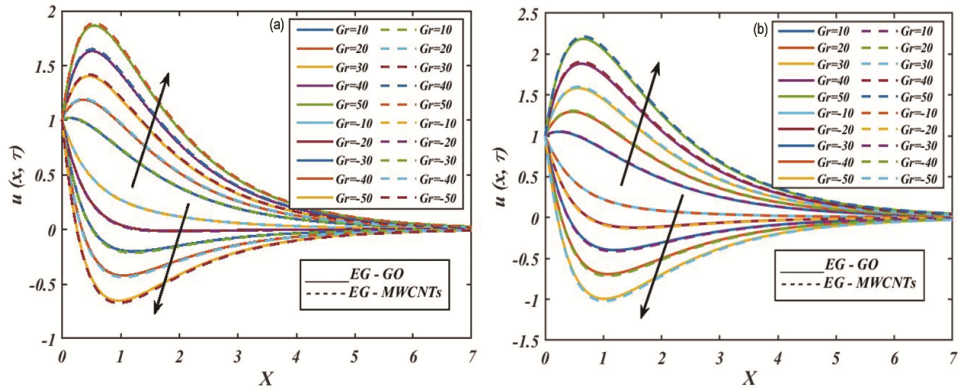

Fig. 8 — Graphical representation of the velocity with various values of Grashof number Gr (a) $\tau = 0.5$ and (b) $\tau = 1.5$ for $\alpha = 0.65$, $\phi = 0.05$, $Pr = 6.2$, $n = 3$, $M = 0.5$ and $\beta = 0.5$

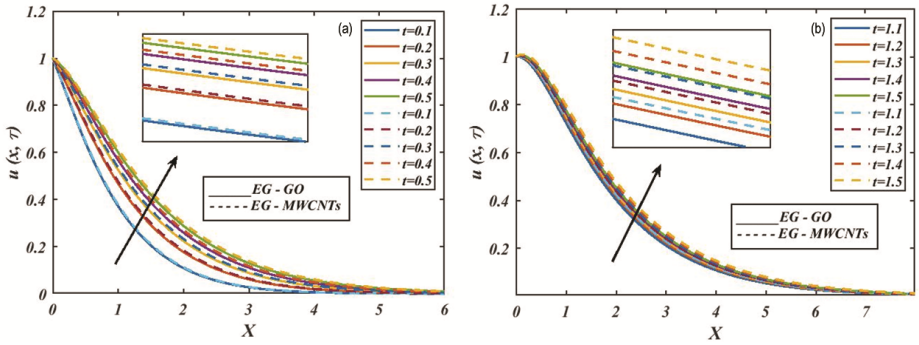

Fig. 9 — Graphical representation of the velocity at different times for $\alpha = 0.65$, $\phi = 0.05$, $Pr = 6.2$, $Gr = 5$, $n = 3$, $M = 0.5$ and $\beta = 0.5$

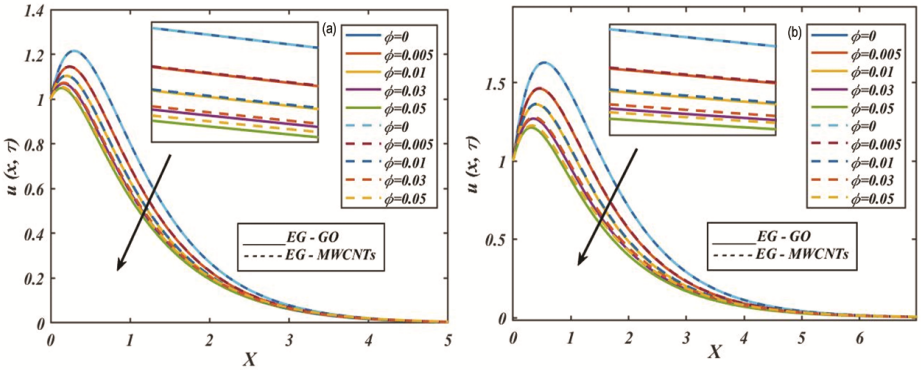

Fig. 10 — Graphical representation of the velocity with distinct values of volume fraction ϕ (a) $\tau = 0.5$ and (b) $\tau = 1.5$ for $\alpha = 0.65$, $Pr = 6.2$, $Gr = 5$, $n = 3$, $M = 0.5$ and $\beta = 0.5$

plate), there is raise in fluid velocity while there is reduction in fluid velocity when the thermal Gr decreases (for heating plate).

Figs. 9(a)-9(b) represents the time influence on velocity distribution. It is seen that as time increases the fluid velocity increases. Figs. 10(a)-10(b) displayed the impact of the volume fraction ϕ at different times $\tau = 0.5$ and 1.5. With an increase in the values of ϕ the velocity decreases, it reveals, the fact that the greater values of volume fraction get reduction in the velocity distribution.

Figs. 11(a)-11(b) displayed the impact of the volume magnetic field parameter M at different times $\tau = 0.5$ and 1.5. It is observed that, with an increase

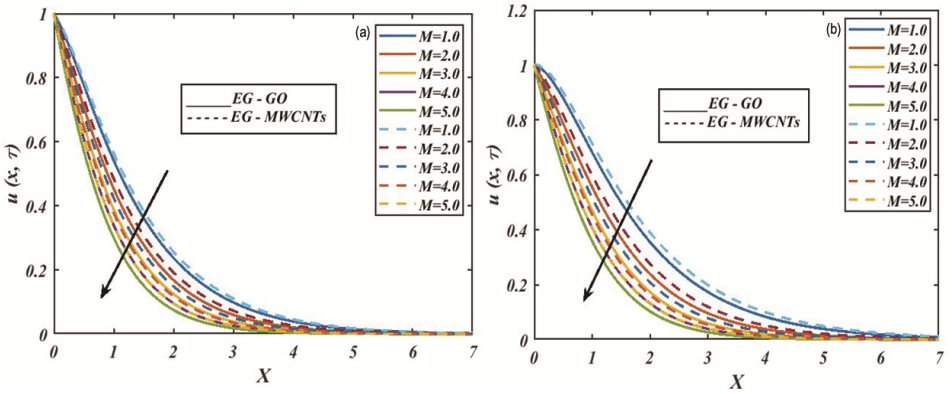

Fig. 11 — Graphical representation of the velocity with distinct values of magnetic field parameter M (a) $\tau = 0.5$ and (b) $\tau = 1.5$ for $\alpha = 0.65$, $Pr = 6.2$, $n = 3, Gr = 5$, $\phi = 0.05$ and $\beta = 0.5$

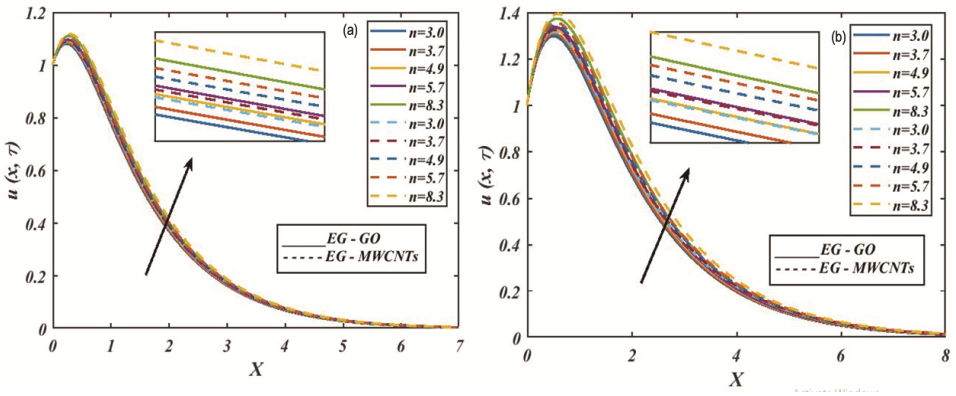

Fig. 12 — Graphical representation of the velocity with distinct shapes of nanoparticles (a) $\tau = 0.5$ and (b) $\tau = 1.5$ for $\alpha = 0.65$, $Pr = 6.2$, $Gr = 5, M = 0.5$, $\phi = 0.05$ and $\beta = 0.5$

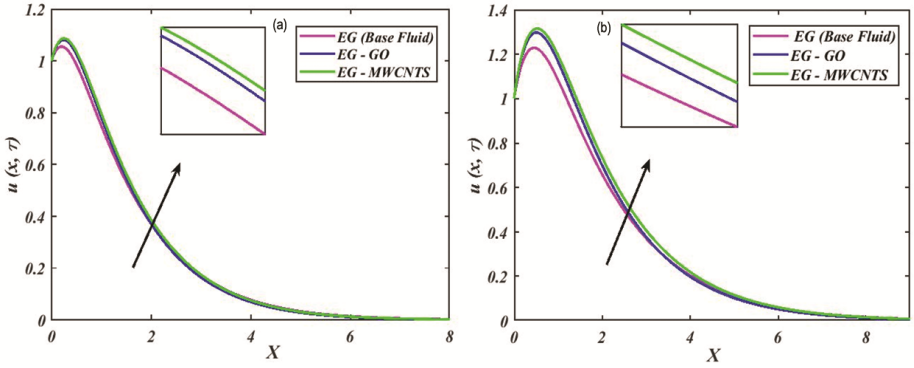

Fig. 13 — Graphical representation of the velocity with distinct nanoparticles (a) $\tau = 0.5$ and (b) $\tau = 1.5$ for $\alpha = 0.65$, $Pr = 6.2$, $Gr = 5$, $n = 3$, $M = 0.5$, $\phi = 0.05$ and $\beta = 0.5$

in the values of M the velocity decreases, which means that the greater values of magnetic field parameter is decreases the velocity distribution.

Figs. 12(a)-12(b) represents the variations of velocity distribution for different shapes of nanoparticles. It is observed that the blade shaped nanoparticles give the effective results for velocity distribution.

A comparison between velocity profiles of pure base fluid Ethylene glycol, nanofluids EG-GO and EG-MWCNT's are presented in Figs. 13(a)-13(b). It is noticed that EG-MWCNT's nanofluids is

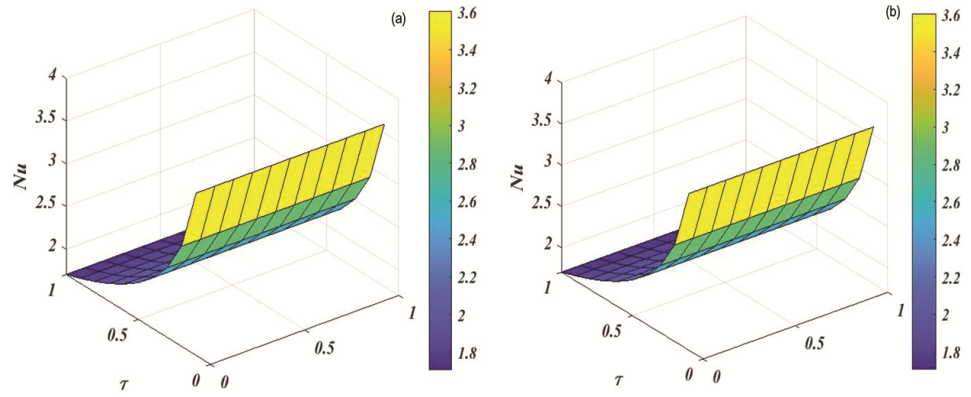

Fig. 14 — 3D graphical representation of Nussult number with distinct nanofluids (a) EG-GO (b) EG-MWCNT's for $\alpha = 0.65$, $\phi = 0.05$, $n = 3$ and $pr = 6.2$

superior than EG-GO. Figs 14(a)-14(b) are the 3D representation of Nussult number.

Conclusion

The Caputo fractional derivative model, flow caused by due to an infinite vertical surface and buoyancy driven, Casson nanofluid with MHD effects are proposed in the current work. The present solution of formulated problem with Caputo derivative is derived by the combination of Fourier sine and Laplace transformations methods. Moreover, the numerical and graphical outcomes exemplify that the fractional thermal transport can predict significant heat transfer enhancements of nanofluids.

Following are the key findings:

- The blade shaped nanoparticles are giving the most effective results by comparing other shaped nano particles to enhance the heat transformation rate.
- We observe that, the temperature of the fluid having dual behaviour when α increases at $\tau = 0.5$ and the temperature of the fluid also increases when an increase in α ($\tau = 1.5$) and $\phi(\tau = 0.5, 1.5)$.
- By comparing the two types of nanoparticles EG-GO and EG- MWCNT's it is observed that EG-MWCNT's gives good results in temperature and velocity distributions.
- The velocity decreases when α increases at $\tau = 0.5$. Also velocity drops when β, ϕ and M raise at $\tau = 0.5$ and 1.5.
- The velocity increases when the fractional parameter α increases at $\tau = 1.5$. The velocity enhances when Gr is raised at $\tau = 0.5$ and 1.5. Also the velocity strengthens when time is increased.
- Nussult number of EG-GO and EG-MWCNT's, increases by elevating Pr and falls by increasing values of τ, α, ϕ.
- Skin frictions of EG-GO and EG-MWCNT's, increase with an enhance in M and ϕ and decreases with an increase in Pr, τ, α, β and Gr.

Nomenclature

Symbol	Quantity	Units
t	: Times	s
g	: Gravitational acceleration	m/s^2
$u(x,t)$	: Fluid Velocity	m/s
$T(x,t)$	: Fluid Temperature	K
T_w	: Wall Temperature	K
σ_{nf}	: Electrical conductivity	$\Omega^{-1} m^{-1}$
T_∞	: Ambient Temperature	K
ρ	: density	Kg/m^3
μ_{nf}	: Dynamic Viscosity	Kg/ms
k_{nf}	: Thermal conductivity of the nanofluid	$W m^{-1} K^{-1}$
γ_{nf}	: Volumetric coefficient of thermal expansion	k^{-1}
C_p	: Specific heat capacity	$J/Kg.K$
B_0	: Magnetic field strength	$(-)$

M	:	Magnetic field parameter	$(-)$
ϕ	:	Volume fraction of nanoparticles	$(-)$
$\theta(x,\tau)$	:	Dimensionless Temperature	$(-)$
$u(x,\tau)$	:	Dimensionless Velocity	$(-)$
q	:	Fourier Transform Parameter	$(-)$
s	:	Laplace Transform Parameter	$(-)$
β	:	Casson Parameter	$(-)$
α	:	Fractional Parameter	$(-)$
Nu	:	Nussult Number	$(-)$
Pr	:	Prandtl Number	$(-)$
C_f	:	Skin friction coefficient	$(-)$
Gr	:	Thermal Grashof Number	$(-)$
erf	:	Gaussian error function	$(-)$
$erfc$	:	Complementary error function	$(-)$

Subscripts

w	:	Conditions on the wall
∞	:	Free stream Conditions
nf	:	Nano material
f	:	Base fluid
p	:	Nano particle

References

1 Sene N, Analytical solutions of a class of fluids models with the Caputo fractional derivative, *Fractal Fract*, 6 (2022) 35.

2 Veeresha P, A Numerical approach to the coupled atmospheric ocean model using a fractional operator, *Math Mod Numer Simul Appl*, 1 (2021) 1.

3 Matin H, Zahra G C, Mohammad M & Maryam K, Comparison study of COD adsorption on bentonite-based nanocomposite materials in landfill leachate treatment: Characterization, isotherms, kinetics and regeneration, *Indian J Chem Technol*, 30 (2023) 370.

4 Subramanyam R A, Govindarajulu K, Anwar B O & Ramachandra P V, Entropy generation on chemically reactive hydromagnetic oscillating flow of third grade nanofluid in a porous channel with Cattaneo-Christov heat flux, *Indian J Chem Technol*, 30 (2023) 9.

5 Uddin M T, Mondal J, Hossain S & Mukhlish M Z, Hydrothermal synthesis of mesoporous TiO_2 nanoparticles for enhanced photocatalytic degradation of organic dye, *Indian J Chem Technol*, 30 (2023) 320.

6 Sene N, Analysis of a four-dimensional hyperchaotic system described by the Caputo–Liouville fractional derivative, *Complex*, 2020 (2020) 1.

7 Qureshi S, Real life application of Caputo fractional derivative for measles epidemiological autonomous dynamical system, *Chaos Solit Fractals*, 134 (2020) 109744.

8 Miller K S & Ross B, An introduction to fractional calculus and fractional equations (New York, A Wiley), (1993).

9 Podlubny, Fractional Differential Equations (New York, Academic Press), (1999).

10 Kilbas A A, Srivastava H M &Trujillo J J, Theory and applications of fractional differential equations, Elsevier, 204 (2006).

11 Yavuz M, Sene N & Yıldız M, Analysis of the influences of parameters in the fractional second-grade fluid dynamics, *J Math*, 10 (2022) 1125.

12 Viera-Martin E, Gómez-Aguilar J F, Solís-Pérez J E, Hernández-Pérez J A & Escobar-Jiménez R F, Artificial neural networks: a practical review of applications involving fractional calculus, *Eur Phys J Spec Top*, 231 (2022) 2059.

13 Sene N, Stokes' first problem for heated flat plate with Atangana–Baleanu fractional derivative, *Chaos Solit Fractals*, 117 (2018) 68.

14 Khalil R, Al-Horani M, Yousef A & Sababheh M, A new definition of fractional derivative, *J Comput Appl Math*, 264 (2014) 65.

15 Elnaqeeb T, Shah N A & Mirza I A, Natural convection flows of carbon nanotubes nanofluids with Prabhakar-like thermal transport, *Math Methods Appl Sci*, (2020) 1. DOI: 10.1002/mma.6584

16 Chen L & Liu Q, Local Fractional Homotopy Perturbation Method for Solving Coupled Sine-Gordon Equations in Fractal Domain, *Fractal Fract*, 6 (2022) 404.

17 Zúñiga-Aguilar C J, Romero-Ugalde H M, Gómez-Aguilar J F, Escobar-Jiménez R F & altierra-Rodríguez V M, Solving fractional differential equations of variable-order involving operators with Mittag-Leffler kernel using artificial neural networks, *Chaos Solit Fractals*, 103 (2017) 382.

18 Inc M, Bouteraa N, Akinlar M A, Benaicha S, Chu Y M, Weber G W & Almohsen B, New positive solutions of nonlinear elliptic PDEs, *Appl Sci*, 10 (2020) 4863.

19 Panda A, Santra S & Mohapatra, Adomian decomposition and homotopy perturbation method for the solution of time fractional partial integro-differential equations, *J Appl Math Comput*, 68 (2022) 2065.

20 Raza A, Khan S U, Farid S, Khan M I, Sun T C, Abbasi A, Khan M I & Malik M K, Thermal activity of conventional Casson nanoparticles with ramped temperature due to an infinite vertical plate via fractional derivative approach, *Case Stud Therm Eng*, 27 (2021) 101191.

21 Al-Qurashi M M, Korpinar Z, Baleanu D & Inc M, A new iterative algorithm on the time-fractional Fisher equation: Residual power series method, *Adv Mech Eng*, 9 (2017) 1687814017716009.

22 Saeed A, Bilal M, Gul T, Kumam P, Khan A & Sohail M, Fractional order stagnation point flow of the hybrid nanofluid towards a stretching sheet, *Sci Rep*, 11 (2021) 20429.

23 Khazayinejad K & Nourazar S S, Space-fractional heat transfer analysis of hybrid nanofluid along a permeable plate considering inclined magnetic field, *Sci Rep*, 12 (2022) 5220.

24 Khan A, Hussain G, Inc M & Zaman G, Existence, uniqueness, and stability of fractional hepatitis B epidemic model, *Chaos*, 30 (2020) 103104.

25 Souayeh B, Abro K A, Siyal A, Hdhiri N, Hammami F, Al-Shaeli M, Alnaim N, Raju S, Alam M W & Alsheddi T, Role of copper and alumina for heat transfer in hybrid nanofluid by using Fourier sine transform, *Sci Rep*, 12 (2022) 11307.

26 Shah N A, Dassios I, El-Zahar E R & Chung J D, An efficient technique of fractional-order physical models involving ρ-Laplace transform, *J Math*, 10 (2022) 816.

27 Asifa, Anwar T, Kumam P, Shah Z & Sitthithakerngkiet K, Significance of shape factor in heat transfer performance of molybdenum-disulfide nanofluid in multiple flow situations; A comparative fractional study, *Molecules*, 26 (2021) 3711.

28 Sheikh N A, Chuan C D L & Khan I, A comprehensive review on theoretical aspects of nanofluids: Exact solutions and analysis, Symmetry, 12 (2020) 725.

29 Anwar T & Kumam P, A fractal fractional model for thermal analysis of GO− NaAlg− Gr hybrid nanofluid flow in a channel considering shape effects, *Case Stud Therm Eng*, 31 (2022) 101828.

30 Islam S, Khan A, Deebani W, Bonyah E, Alreshidi N A & Shah Z, Influences of Hall current and radiation on MHD micropolar non-Newtonian hybrid nanofluid flow between two surfaces, *AIP Adv*, 10 (2020) 055015.

31 Khalid A, Khan I, Khan A & Shafie S, Unsteady MHD free convection flow of Casson fluid past over an oscillating vertical plate embedded in a porous medium, *Eng Sci Technol Int J*, 18 (2015) 309.

32 Bhatta D P, Optically thick radiating free convective MHD nanofluid flow over an exponentially accelerated plate, *Karbala Int J Mod Sci*, 6 (2020) 9.

33 Hanif H & Shafie S, Impact of Al_2O_3 in electrically conducting mineral oil-Based Maxwell nanofluid: Application to the petroleum industry, *Fractal Fract*, 6 (2022) 180.

34 Sene N, Second-grade fluid with Newtonian heating under Caputo fractional derivative: Analytical investigations via Laplace transforms, *Math Mod Numer Simul Appl*, 2 (2022) 13.

35 Anwar M S, Ahmad R T, Shahzad T, Irfan M & Ashraf M Z, Electrified fractional nanofluid flow with suspended carbon nanotubes, *Comput Math with Appl*, 80 (2020) 1375.

36 Ali G, Ali F, Khan A, Ganie A H & Khan I, A generalized magnetohydrodynamic two-phase free convection flow of dusty Casson fluid between parallel plates, *Case Stud Therm Eng*, 29 (2022) 101657.

37 Arif M, Ali F, Sheikh N A, Khan I & Nisar K S, Fractional model of couple stress fluid for generalized Couette flow: A comparative analysis of Atangana–Baleanu and Caputo–Fabrizio fractional derivatives, *IEEE Access*, 7 (2019) 88643.

38 Souayeh B & Abro K A, Thermal characteristics of longitudinal fin with Fourier and non-Fourier heat transfer by Fourier sine transforms, *Sci Rep*, 11 (2021) 20993.

39 Zubair T, Usman M, Sooppy N K, Khan I, Ghamkhar M & Ahmad M, Nicholson scheme to examine the fractional-order unsteady nanofluid flow of free convection of viscous fluids, *PloS one*, 17 (2022) e0261860.

40 Javed F, Riaz M B, Iftikhar N, Awrejcewicz J & Akgül A, Heat and mass transfer impact on differential type nanofluid with carbon nanotubes: a study of fractional order system, *Fractal Fract*, 5 (2021) 231.

41 Reyaz R, Mohamad A Q, Lim Y J, Saqib M & Shafie S, Analytical solution for impact of Caputo-Fabrizio fractional derivative on MHD casson fluid with thermal radiation and chemical reaction effects, *Fractal Fract*, 6 (2022) 38.

42 Raza A, Khan U, Zaib A, Mahmoud E E, Weera W, Yahia I S & Galal A M, Applications of Prabhakar-like fractional derivative for the solution of viscous type fluid with Newtonian heating effect, *Fractal Fract*, 6 (2022) 265.

43 Asjad M I, Usman M, Ali A, Awrejcewicz J & Bednarek M, Insight into the dynamics of fractional Maxwell nano-fluids subject to entropy generation, Lorentz force and heat source via finite difference scheme, *Nanomaterials*, 12 (2022) 1745.

44 Sene N, A numerical algorithm applied to free convection flows of the Casson fluid along with heat and mass transfer described by the Caputo derivative, *Adv Math Phys*, (2021) 1-11.

45 Aman S, Khan I, Ismail Z, Salleh M Z & Tlili Z, A new Caputo time fractional model for heat transfer enhancement of water based graphene nanofluid: An application to solar energy, *Results Phys*, 9 (2018) 1352.

46 Zhang J, Raza A, Khan U, Ali Q, Zaib A, Weera W & Galal A M, Thermophysical Study of Oldroyd-B Hybrid nanofluid with sinusoidal conditions and permeability: A Prabhakar fractional approach, *Fractal Fract*, 6 (2022) 357.

47 Kumam P, Tassaddiq A, Watthayu W, Shah Z & Anwar T, Modeling and simulation based investigation of unsteady MHD radiative flow of rate type fluid; a comparative fractional analysis, *Math Comput Simul*, 201 (2022) 486.

48 Arif M, Kumam P, Kumam W & Mostafa Z, Heat transfer analysis of radiator using different shaped nanoparticles water-based ternary hybrid nanofluid with applications: A fractional model, *Case Stud Therm Eng*, 31 (2022) 101837.

49 Chu Y M, Nisar K S, Khan U, Daei K H, Malaver M, Zaib A & Khan I, Mixed convection in MHD water-based molybdenum disulfide-graphene oxide hybrid nanofluid through an upright cylinder with shape factor, *Water*, 12 (2020) 1723.

50 Akbar Y, Akram U, Aun M A, Afsar H & Javed M W, MHD peristaltic transportation of radiative MWCNT-Ag/$C_2H_6O_2$ hybrid nanofluid with variable characteristics, *Today Commun*, 28 (2021) 102681.